A novel glideosome-associated protein S14 coordinates sporozoite gliding motility and infectivity in mosquito and mammalian hosts

Ankit Ghosh[1#], Aastha Varshney[1#], Sunil Kumar Narwal[1], Nirdosh[1,2], Sachin Gaurav[3], Roshni Gupta[1], Shakil Ahmed[3] and Satish Mishra[1, 2*]

[1]Division of Molecular Microbiology and Immunology, CSIR-Central Drug Research Institute, Lucknow 226031, India.

[2]Academy of Scientific and Innovative Research (AcSIR), Ghaziabad 201002, India.

[3]Division of Biochemistry and Structural Biology, CSIR-Central Drug Research Institute, Lucknow 226031, India.

[*]Corresponding author: Satish Mishra

E-mail: satish.mishra@cdri.res.in

ORCID ID: 0000-0002-8942-6416

Tel. (+91) 522-2772450*4529

[#]Contributed equally to this work.

Abstract

Plasmodium sporozoites are the infective forms of the malaria parasite in the vertebrate host. Gliding motility allows sporozoites to migrate and invade the salivary gland and hepatocytes. Invasion is powered by an actin-myosin motor complex linked to glideosome. However, the gliding complex and the role of several glideosome-associated proteins (GAPs) are poorly understood. In silico analysis of a novel protein, S14, which is uniquely upregulated in salivary gland sporozoites, suggested its association with glideosome-associated proteins. We confirmed *S14* expression in sporozoites using real-time PCR. Further, the *S14* gene was endogenously tagged with 3XHA-mCherry to study expression and localization. We found its expression and localization on the inner membrane of sporozoites. By targeted gene deletion, we demonstrate that S14 is essential for sporozoite gliding motility, salivary gland, and hepatocyte invasion. The gliding and invasion-deficient *S14* KO sporozoites showed normal expression and organization of IMC and surface proteins. Using in silico and the yeast two-hybrid system, we showed the interaction of S14 with the glideosome-associated proteins GAP45 and MTIP. Together, our data show that S14 is a glideosome-associated protein and plays an essential role in sporozoite gliding motility, which is critical for the invasion of the salivary gland, hepatocyte, and malaria transmission.

Key words: Plasmodium, sporozoites, S14, gliding motility, inner membrane complex, glideosome, invasion

Introduction

The *Plasmodium* life cycle alternates between a mosquito and a mammalian host, which involves invasive and replicative stages. When a mosquito probes for the blood meal in an infected human, it ingests the gametocytes, which develop further into gametes that fuse to form the zygote. The zygote transforms into ookinetes, producing hundreds to thousands of oocysts in the mosquito midgut. Following oocyst rupture, sporozoites are released in the hemolymph and further invade the salivary gland (Klug & Frischknecht, 2017; Douglas *et al*, 2015). Sporozoites transform into liver stages after transmission to the human host, forming thousands of merozoites that initiate the erythrocytic cycle (Ripp *et al*, 2021; Prudêncio *et al*, 2006). Sporozoites are highly motile cells and rely on gliding motility to travel through different host species. The gliding motility is powered by the inner membrane complex (IMC) anchored actomyosin machinery termed the glideosome (Baum *et al*, 2008; Kono *et al*, 2013). The motor is located in the IMC, separating the flattened alveolar sacs and parasite plasma membrane (PPM) (Gould *et al*, 2011). The gliding-associated proteins (GAPs) tether MyoA to the IMC and hold the PPM and the IMC together (Boucher & Bosch, 2015). These transmembrane proteins connect the submembrane motor to the extracellular environment (King, 1988)

Plasmodium sporozoites can invade target cells in the mosquito and the mammalian hosts and many proteins that have been implicated during this process are expressed specifically in sporozoites. Thrombospondin-related anonymous protein (TRAP) was found to be the first protein involved in sporozoite gliding motility and host cell invasion. TRAP mutant sporozoites failed to invade the salivary gland, and hemolymph sporozoites were nonmotile (Sultan *et al*, 1997). TRAP cytoplasmic tails incorporate a C-terminal tryptophan residue that is crucial for interaction with aldolase that connects with an actin-myosin-based motor

(Heintzelman, 2015; Buscaglia *et al*, 2003). S6 is also a TRAP family adhesion, and by disruption, its role has been implicated in parasite adhesion and gliding motility (Steinbuechel & Matuschewski, 2009). The other proteins involved in parasite motility and host cell invasion include MAEBL (Kariu *et al*, 2002; Saenz *et al*, 2008), TLP (Heiss *et al*, 2008), the rhoptry-resident proteins TRSP (Labaied *et al*, 2007), RON4 (Giovannini *et al*, 2011), GEST (Talman *et al*, 2011), TREP/UOS3 (Mikolajczak *et al*, 2008; Combe *et al*, 2009), the GPI-anchored circumsporozoite protein (CSP) of the sporozoite and the small solute transporter PAT (Kehrer *et al*, 2016) and claudin-like apicomplexan microneme protein (CLAMP) (Loubens *et al*, 2023). The individual functions of these proteins are known. However, how they interact with each other to coordinate gliding motility and invasion is poorly understood.

These proteins are specific to sporozoites; however, several overlapping proteins are known that function in both merozoites and sporozoites. Proteins such as GAP-40, -45, and -50 together with myosin A tail domain interacting protein (MTIP) cluster MyoA with IMC (Poulin *et al*, 2013; Daher & Soldati-Favre, 2009). In *P. falciparum*, the peripheral protein GAP45 is myristoylated and palmitoylated, possibly required for membrane targeting (Rees-Channer *et al*, 2006). GAP45 in *Toxoplasma gondii* is involved in the recruitment of the motor complex (Frénal *et al*, 2010). *Pf*GAP50 is a transmembrane protein that anchors the invasion machinery in the inner membrane complex (Baum *et al*, 2006; Yeoman *et al*, 2011). In *T. gondii*, GAP45 and GAP50 form a complex with MyoA and its light chain, MLC1.

While the glideosome and many surface proteins have been studied and found essential for gliding motility and invasion, the role of gliding-associated proteins is unexplored. To identify a novel GAP, we performed bioinformatic studies on S14, whose transcripts were

highly upregulated in sporozoites in a suppressive subtraction hybridization study (Kaiser *et al*, 2004). Similar to GAP45 and -50, we found that S14, while not containing transmembrane domains or signal peptides, is predicted to be secreted via the nonclassical pathway. It also contains a predicted palmitoylation signal, possibly indicating its membrane targeting (Table S1). In this study, we investigated the role of S14 in the *P. berghei* life cycle. We demonstrate that S14 is an IMC protein interacting with the glideosome-associated proteins MTIP and GAP45. We disrupted the gene and found that S14 is essential for sporozoite gliding motility, host cell invasion, and malaria transmission.

Results

In silico studies show that S14 is secreted via a nonclassical pathway

A study comparing transcriptome differences between sporozoites and merozoites using suppressive subtraction hybridization found several genes highly upregulated in sporozoites and named them 'S' genes (Kaiser *et al*, 2004). We narrowed it down to a candidate named S14, which lacked signal peptide and transmembrane domains. In silico studies revealed that *Pb*S14 is a protein conserved in all *Plasmodium* species and has no similarity in other organisms (Figure S1). The identity matrix showed that the *Pb*S14 protein is highly conserved among all Plasmodia (Table S2). To understand its possible function, we analyzed several sporozoite-specific proteins. We found that gliding-associated proteins GAP45 and GAP50 show similar properties and contain a palmitoylation signal, secreted via the nonclassical pathway and localized to the inner membrane complex (Rees-Channer *et al*, 2006). Next, we performed bioinformatic analysis to check whether S14 is targeted to the inner membrane by a nonclassical secretion pathway. We analyzed the presence of transmembrane domains, prediction of palmitoylation signals, and interactions as previously described (Boucher and Bosch, 2015). We found that S14, while not containing

126 transmembrane domains or signal peptides, is predicted to be secreted via the nonclassical
127 pathway. It also contains a predicted palmitoylation signal, possibly indicating its membrane
128 targeting (Table S1). The nonclassical secretion pathway, which depends on palmitoylation
129 and myristoylation, has been identified in most eukaryotes (Rabouille et al. 2012), including
130 *P. falciparum* (Moskes et al. 2004).
131
132 **S14 is expressed and localized on the membrane of sporozoites**
133 We started our study by validating the transcripts of S14 in different stages of the parasites
134 using quantitative real-time PCR. We found that S14 was predominantly expressed in midgut
135 and salivary gland sporozoites (Figure 1A). To further investigate whether S14 transcripts are
136 translated, we endogenously tagged the *S14* gene with 3XHA-mCherry using double
137 crossover homologous recombination (Figure S2A). The correct site-specific integration was
138 confirmed by diagnostic PCR (Figure S2B). We initiated the mosquito cycle and found that
139 the C-terminal tag did not affect parasite development throughout the life cycle stages (Figure
140 S2C and S2D). We monitored live mCherry expression throughout the parasite life cycle
141 stages. S14-3XHA-mCherry expression was observed in sporozoites but not in the blood and
142 liver stages (Figure 1B and C). Analysis of the mCherry pattern on sporozoites revealed
143 localization on the membrane of the sporozoites (Figure 1D). Furthermore, IFA with anti-
144 CSP and anti-mCherry antibodies confirmed S14 localization on the membrane (Figure 1E).
145 Expression of the S14-3XHA-mCherry fusion protein (~66.5 kDa) was also confirmed by
146 Western blotting using an anti-mCherry antibody. The appearance of an extra band with
147 higher molecular weight in immunoblotting was possibly due to the palmitoylation of S14
148 (Figure 1F). Similar electromobility shifts of GAP45 due to the palmitoylation have been
149 reported (Frénal *et al*, 2010). These results indicate that S14 is a sporozoite-specific
150 membrane protein.

151

152 **_S14_ KO sporozoites egress from the oocyst normally while failing to invade the salivary**
153 **gland**

154 To investigate the role of S14 in the *P. berghei* life cycle, we disrupted the gene by double-
155 crossover homologous recombination (Figure S3A). The drug-resistant parasites expressing
156 GFP indicated successful transfection (Figure S3B). We obtained clonal lines of the KO
157 parasites by limiting dilution of the parasites, integration, and the absence of WT locus was
158 confirmed by diagnostic PCR (Figure S3C). Finally, two *S14* KO clonal lines were confirmed
159 by Southern blotting, which showed the modified locus in the KO parasites (Figure S3D).
160 The S14-complemented parasite line was also generated to check the specificity of the
161 phenotype (Figure S3E). First, a new *S14* KO parasite with yFCU was generated, and then an
162 S14 expression cassette consisting of the 5'UTR, ORF, and 3'UTR was amplified and
163 transfected into *S14* KO (yFCU) parasites. After recombination, the WT locus was amplified
164 in S14 comp parasites (Figure S3F). Next, we checked the propagation of the asexual
165 intraerythrocytic cycle of KO parasites, which was comparable to that of WT GFP parasites
166 (Figure S4). To analyze the phenotype of *S14* KO parasites in mosquito stages, we
167 transmitted them to mosquitoes by allowing them to probe for a blood meal. We observed the
168 mosquito midgut and salivary glands on day 14 and day 19 post-blood meal. We found that
169 oocyst formation and development of sporozoites were comparable to those of WT GFP
170 parasites (Figure 2A-D). However, no sporozoite-associated GFP signals were observed in
171 salivary glands, and the number of salivary gland sporozoites per mosquito was severely
172 reduced (Figure 2E and F). Genetic complementation of the KO parasites restored salivary
173 gland sporozoite numbers to a level similar to WT GFP parasites (Figure 2F). To investigate
174 whether the KO sporozoites failed to egress from the oocyst or could not invade the salivary
175 gland. We counted the sporozoite numbers in the mosquito hemolymph. We found a higher

accumulation of hemolymph sporozoites in KO-infected mosquitoes than in WT GFP-infected mosquitoes (Figure 2G), suggesting that mutant sporozoites failed to invade the salivary gland. These results indicate that mutant sporozoites egress from the oocysts normally but fail to invade salivary glands.

S14 is essential for malaria transmission

To evaluate the ability of salivary gland sporozoites to transmit malaria, infected mosquitos were allowed to inoculate sporozoites in C57BL/6 mice by enabling them to probe for the blood meal. We found that mice inoculated with WT GFP or S14 comp sporozoites became patent on day 3, whereas *S14* KO sporozoites failed to initiate blood-stage infection (Table 1). Next, we checked whether this in vivo infectivity defect was due to negligible salivary gland sporozoite load or mutant sporozoites failed to infect mice. For this, we intravenously inoculated C57BL/6 mice with 5,000 hemolymph sporozoites and found that all the mice inoculated with KO sporozoites failed again to initiate blood-stage infection (Table 1). To determine the stage-specific defect, we performed in vitro assays. First, we infected HepG2 cells with hemolymph sporozoites and observed EEF development at 40 hpi. In three independent experiments, we found EEFs in culture inoculated with WT GFP sporozoites but not in the KO-infected cells (Figure 3A and S5A). Next, we checked the invasion capacity of *S14* KO hemolymph sporozoites using double immunostaining, which differentiates outside vs inside sporozoites (Rénia *et al*, 1988). *S14* KO sporozoites showed a complete failure to invade hepatocytes (Figure 3B and S5B), explaining the inability to establish an infection in mice. Next, we performed a development assay to check the mutant sporozoite transformation ability into a bulb-like structure. For this, we incubated the mutant sporozoites in a transformation medium for 4 h. We found that *S14* KO sporozoites retain the ability to transform into bulb-like structures (Figure 3C and D). These data demonstrate that *S14* KO

sporozoites lost infectivity to mammalian hosts due to the inability of sporozoites to invade cells.

S14 localizes on the inner membrane and is essential for parasite gliding motility

Invasion-deficient *S14* KO sporozoites indicate that either S14 interacts with host receptors or cannot generate power to invade cells. As S14 lacks a signal sequence and transmembrane domain, we analyzed whether S14 is present on the outer or inner membrane. We treated S14-3XHA-mCherry hemolymph sporozoites with Triton X-100 to remove the outer membrane. The Triton X-100-treated and untreated sporozoites were immunostained with anti-CSP and anti-mCherry antibodies. The CSP signal was lost in Triton X-100-treated sporozoites, whereas the S14-3XHA-mCherry signal was retained (Figure 4A). Western blotting confirmed the IFA result, which detected the mCherry signal in Triton X-100-treated sporozoites (Figure 4B). To further confirm the inner membrane localization of S14, we generated antibodies against two IMC proteins MTIP (Bergman *et al*, 2003) and GAP45 (Gaskins *et al*, 2004), and performed IFA. The MTIP and GAP45 signals were retained in Triton X-100-treated sporozoites and colocalized with the mCherry signal (Figure 4A). This result indicates that S14 is present within the inner membrane of sporozoites. *Plasmodium* parasites actively invade host cells, powered by gliding motility (Frénal *et al*, 2017). Next, we checked the gliding motility of WT GFP and *S14* KO hemolymph sporozoites. WT GFP sporozoites glided normally, whereas *S14* KO sporozoites were found to be nonmotile (Figure 4C). We counted the sporozoites associated with or without trails to quantify the percentage of gliding sporozoites. Approximately 53% of WT GFP sporozoites were associated with trails, whereas no trails associated with sporozoites were observed in *S14* KO

(Figure 4D). These data demonstrate that S14 is an IMC protein that powers the sporozoite's gliding motility.

In silico docking revealed the interaction of S14 with GAP45 and MTIP

The gliding phenotype of the S14 KO and its localization on IMC prompted us to investigate the association of S14 with glideosome-associated proteins. We chose two IMC-localized proteins, MTIP (Bergman *et al*, 2003) and GAP45 (Gaskins *et al*, 2004), for the interaction studies. We started with bioinformatic studies to check the interaction of S14 with MTIP and GAP45. Structural models of MTIP, GAP45 and S14 were obtained and docking was performed (Figure S6). The ClusPro Docking server binding energy of MTIP-GAP45, S14-GAP45, and S14-MTIP were -1216 Kcal/mol, -898.6 Kcal/mol, and -1024.6 Kcal/mol, respectively. Further, we performed the docking using the HDOCK server for the receptor-ligand interface (Figure S7). The set cut-off confidence score was 0.5 and the confidence score for MTIP-GAP45, S14-GAP45 and S14-MTIP interactions were 0.6400, 0.6976 and 0.7235, respectively. These results indicated that MTIP-GAP45 and S14-GAP45 would possibly bind and S14-MTIP are likely to bind. Furthermore, we analyzed protein-protein interaction using HADDOCK server and obtained top Z score clusters were submitted to PDBe_PISA, which revealed interacting residues interface through hydrogen bonding and salt bridge residues. The receptor-ligand interface residues less than 3Å were visualized using Pymol (Figure 5). The respective receptor-ligand interface are given in Tables S3 and S4. The binding energies and residue interface studies indicate that S14 interact with GAP45 and MTIP.

S14 interacts with GAP45 and MTIP in Yeast two-hybrid assay

To further confirm the in-silico interaction results, yeast two-hybrid assay was performed. For this, *P. berghei* S14 was cloned into pAS2, and the MTIP and GAP45 genes were cloned into pGAD-C1 yeast two-hybrid vectors. The plasmid containing the *S14* gene was cotransformed with MTIP or GAP45 genes in the *S. cerevisiae* strain PJ69-4A. Interaction studies were performed using LacZ and HIS3 as reporters and revealed a positive interaction of S14 with the MTIP and GAP45 proteins, as these cells were able to grow on SD-Trp-Leu-His plates containing 10 and 25 mM 3-AT (Figure 6). Furthermore, these cells also gave blue color on plates containing X-gal (Figure 6), indicating a positive interaction of the S14 protein with the MTIP and GAP45 proteins. In contrast, a negative control containing two unrelated proteins could not grow on 3-AT plates and did not give a blue color on the X-gal plate. This data confirmed the interaction of S14 with GAP45 and MTIP.

S14 coordinate gliding motility without affecting IMC and surface protein expression and localization

Plasmodium sporozoites exhibit a substrate-dependent gliding motility for which surface and IMC proteins are employed. We analyzed the expression and organization of two IMC proteins, MTIP and GAP45, and two surface proteins, CSP and TRAP in *S14* KO sporozoites. Immunostaining revealed an intact IMC and surface organization in *S14* KO sporozoites (Figure 7). This data indicate that S14 performs gliding-specific function and does not affect the organization of IMC and surface proteins.

Discussion

This study identified a novel *Plasmodium* protein, S14, which lacks signal peptide and transmembrane domains. However, it contains a palmitoylation signal, secreted via the nonclassical pathway and localized to the inner membrane complex. We found that S14 is a

gliding-associated protein with a core function in gliding motility and host cell invasion. Deletion of S14 resulted in the accumulation of a higher number of sporozoites in hemolymph, which failed to invade the salivary gland and hepatocytes. The inability of *S14* KO sporozoites to invade the host cell was due to impaired gliding motility. Furthermore, we show that S14 interacts with the glideosome-associated proteins GAP45 and MTIP. Overall, these results indicate a central role for S14 in coordinating gliding motility and invasion of *Plasmodium* sporozoites.

We propose that S14 works with GAP45 and MTIP, facilitating gliding motility. It is possible that S14 connects GAP45 and MTIP or could act entirely independently. Both scenarios are possible because the details of this complex are not known. Similar to S14, several parasite proteins play a role in the gliding motility and invasion of both mosquito and human hosts, such as surface protein TRAP (Sultan et al., 1997) and claudin-like apicomplexan microneme protein (CLAMP) (Loubens *et al*, 2023); however, MAEBL was found to be important for attachment to the salivary gland surface and did not affect sporozoite motility and infectivity to the vertebrate host (Kariu *et al*, 2002). S14 is not a surface protein with an extracellular domain, and its host cell invasion defect was due to impaired gliding. Cellular transmigration and host cell invasion are prerequisites for gliding motility. Several sporozoite proteins, such as SPECT, SPECT2, and PLP1, differ from S14, as they invade the host cell usually with a deficiency in cell traversal (Ishino *et al*, 2004, 2005b; Risco-Castillo *et al*, 2015). Surface proteins such as P36 and P52 show normal gliding motility and cell traversal and play a role in host cell invasion by interacting with host cell receptors (Ishino *et al*, 2005a; Manzoni *et al*, 2017; Arredondo *et al*, 2018).

The parasite gliding machinery consists of the atypical myosin MyoA, MTIP, and ELC1, the glideosome-associated proteins GAP40 and GAP45, and the transmembrane protein GAP50 (Bergman *et al*, 2003; Frénal *et al*, 2010). This MyoA interacts with F-actin, which connects with surface proteins through aldolase (Sultan *et al*, 1997; Jewett & Sibley, 2003; Huynh & Carruthers, 2006). In *T. gondii*, GAP45 plays a vital role in maintaining the close association of the IMC to the plasma membrane (Frénal *et al*, 2010). GAP45 also interacts with GAP50 through its C-terminal region, supporting its function as the anchor of the motor complex in the IMC. We selected GAP45 and MTIP for interaction studies with S14 because MyoA was lost upon the downregulation of MTIP. Furthermore, MTIP was found to be reduced in GAP45 knockdown (Sebastian *et al*, 2012).

Deletion of S14 resulted in the accumulation of a higher number of sporozoites in hemolymph, indicating the dispensable role of S14 during the egress of sporozoites from oocysts. The conditional deletion of GAP45 during *P. falciparum* asexual blood stages revealed its role in the invasion but not in egress. These results indicate that a functional motor complex is not required for egress from RBCs, which plays a critical role in invasion (Perrin *et al*, 2018). GAP40 and GAP50 and members of the GAPM family play critical roles in the biogenesis of IMCs during intracellular replication. Parasites lacking GAP40 or GAP50 start replication but fail to complete it, implicating a structural role in maintaining the stability of the developing IMC during replication (Harding *et al*, 2016). It was shown that IMC is critical for the anchorage and stabilization of the glideosome (Opitz & Soldati, 2002) and is required during the invasion of the host cell (Bargieri *et al*, 2013; Egarter *et al*, 2014; Togbe *et al*, 2008; Meissner *et al*, 2013). We hypothesize that S14 possibly plays a structural role and maintains the stability of IMC required for the activity of motors during gliding and invasion. S14 deletion does not affect GAP45, MTIP, CSP and TRAP expression and

localization, suggesting that it performs motor-related functions only. These results indicate that the S14-associated IMC complex possibly exists in sporozoites and coordinates gliding motility (Figure 8); however, the link between S14, GAP45, and MTIP requires further investigation.

Material and methods

Parasites, Mosquitos, and Mice

Plasmodium berghei ANKA (MRA 311) and *P. berghei* ANKA GFP (MRA 867 507 m6cl1) were obtained from BEI resources, USA. *Anopheles stephensi* mosquitos were reared at 28°C and 80% relative humidity and kept under a 12 h light/dark cycle as previously described (Gupta *et al*, 2020). Swiss albino and C57BL/6 mice were used for parasite infections. All animal procedures were approved by the Institutional Animal Ethics Committee at CSIR-Central Drug Research Institute, India (IAEC/2013/83).

Protein association prediction for PbS14

Using the "guilt-by-association" principle of prediction, we chose to study the following properties of existing glideosome components along with S14: (1) Classical pathway secretion using the signal peptide (SignalP). (2) Nonclassical pathway secretion (SecretomeP). (3) Presence of transmembrane domains (TMHMM). (4) Presence of a potential palmitoylation site (CSS-Palm). (5) Known associations from the literature. This is a similar association prediction method as employed by the STRING database. These properties were chosen on the rationale that the presence of these signals ascertains protein targeting to different cellular membranes. Associating these characteristics with the known glideosome proteins and their interactions (Boucher & Bosch, 2015), we could select a few

348 glideosome components to check for physical interactions using in-silico studies and yeast
349 two-hybrid assay.
350
351 **S14 expression analysis by RT–qPCR**
352 For the absolute quantification of *S14* transcripts, a standard was generated by amplifying a
353 120 bp fragment within the *S14* ORF (PBANKA_0605900) using primers 1001/1002
354 (primers are given in Table S5). The amplified product was cloned into the pCR 2.1-TOPO
355 vector. For the normalization of transcripts, Hsp70 was used (Choudhary *et al*, 2019). Total
356 RNA was isolated from blood stage schizonts (Schz), liver stages (LS), midgut (MG), and
357 salivary gland (SG) sporozoites using TRIzol reagent (Takara Bio, Japan) and an RNA
358 isolation kit (Genetix, India) following the manufacturers' instructions. cDNA was prepared
359 by reverse transcription using a Superscript cDNA synthesis kit. Real-time PCR was carried
360 out using SYBR green reagent (Takara Bio, Japan), and the ratio of transcript numbers of *S14*
361 and *Hsp70* was used to determine the copy number.
362
363 **Generation of S14-3XHA-mCherry transgenic parasites**
364 For the endogenous tagging of S14 with 3XHA-mCherry, two fragments, F1 (0.74 kb) and F2
365 (0.65 kb), were amplified using 1010/1011 and 1005/1006 and cloned into plasmid pBC-
366 3XHA-mCherry-hDHFR at *Xho*I/*Bgl*II and *Not*I/*Asc*I, respectively. The plasmid was
367 linearized using *Xho*I/*Asc*I and transfected into *P. berghei* ANKA schizonts as previously
368 described (Janse *et al*, 2006). Correct 5' and 3' site-specific integration was confirmed by
369 diagnostic PCR using primers 1007/1392 and 1215/1008, respectively (primers are given in
370 Table S5). The clonal lines were obtained by limiting dilution of the parasites and analyzed
371 for expression and localization.
372

373 **Generation of *S14* KO and complemented parasites**

374 *P. berghei S14* (PBANKA_0605900) was disrupted by double-crossover homologous
375 recombination. For this, two fragments, F3 (0.73 kb) and F4 (0.637 kb), were amplified using
376 *P. berghei* ANKA genomic DNA with primers 1003/1004 and 1005/1006, respectively. The
377 fragments F3 and F4 were cloned sequentially into the pBC-GFP-hDHFR vector at *Xho*I/*Cla*I
378 and *Not*I/*Asc*I, respectively, and finally linearized with *Xho*I/*Asc*I and transfected into *P.*
379 *berghei* schizonts (Janse *et al*, 2006). The drug-resistant GFP-expressing parasites were
380 confirmed for 5' and 3' site-specific integrations using primers 1007/1225 and 1215/1008,
381 respectively (primers are given in Table S5). To generate an *S14* KO complemented parasite
382 line, another *S14* KO parasite line was generated with the hDHFR:yFCU selection cassette. A
383 fragment consisting of the S14 5'UTR, ORF, and 3'UTR was amplified using primers
384 1003/1006 and transfected into *S14* KO parasites. Parasites containing restored S14 loci were
385 selected by negative selection using a 5-fluorocytosine (5-FC) drug (Sigma, USA) as
386 previously described (Srivastava & Mishra, 2022). The clonal lines were obtained by limiting
387 dilution of the parasites, and the absence of *S14* ORF was confirmed using primers
388 1010/1011. Furthermore, two clonal lines were also confirmed by Southern blotting as
389 described previously (Narwal *et al*, 2022). Fragment F3 was used as a probe to detect the
390 band in Southern blot.

391

392 **Phenotypic characterization of *S14* KO parasites**

393 The *S14* KO clonal lines were first analyzed for asexual blood-stage propagation, and for
394 this, 200 µl of iRBCs with 0.2% parasitemia was intravenously injected into a group of mice.
395 Parasitemia was monitored daily by Giemsa staining of blood smears. Next, we initiated
396 infection with KO parasites in *Anopheles stephensi* mosquitos as previously described
397 (Narwal *et al*, 2022). On days 14 and 19, midgut and salivary glands were observed for

398 infection, and sporozoite numbers were counted. The hemolymph sporozoites were collected
399 and counted as previously described (Mastan *et al*, 2017).
400
401 **In vivo infectivity**
402 To determine the in vivo infectivity of KO sporozoites, C57BL/6 mice were either infected
403 by mosquito bite or by intravenously injecting hemolymph sporozoites. For the bite
404 experiment, ten mosquitos per cage were used. The appearance of parasites in the blood was
405 observed by making Giemsa-stained blood smears.
406
407 **In vitro infectivity of sporozoites**
408 The in vitro infectivity of sporozoites was tested by infecting HepG2 cells as previously
409 described (Narwal *et al*, 2022). Fifty thousand cells/well were seeded in 48-well plates
410 containing sterilized coverslips pretreated with collagen. Hemolymph sporozoites (10,000
411 sporozoites/well for the invasion assay or 5,000 sporozoites/well for EEF development) were
412 added to the HepG2 monolayers, and the plate was centrifuged at 310 g for 4 min and
413 incubated at 37°C in a CO2 incubator. The culture was fixed using 4% PFA at 1 hpi for the
414 invasion assay and 40 hpi for the EEF development assay.
415
416 **Transformation of sporozoites into early EEFs without host cells**
417 WT GFP and *S14* KO hemolymph sporozoites were incubated in a medium containing
418 DMEM with 2 mM L-glutamine, 4.5 g/liter glucose, and supplemented with 10% FBS
419 (Sigma, USA), 500 U/ml penicillin–streptomycin, (Thermo Fisher Scientific, USA) and 1.25
420 µl/ml fungizone as previously described (Kaiser *et al*, 2003). The sporozoites were incubated
421 at 37°C in a CO2 incubator for 4 hrs and then fixed using 4% PFA.
422

423 **Generation of anti-MTIP and anti-GAP45 antibodies**

424 Affinity-purified polyclonal rabbit antibodies against *P. berghei* MTIP and GAP45 were
425 developed by GenScript Inc., Piscataway, NJ, against the peptide sequences
426 CVNKDDRKIYFDEKS and CHKYENDSDKLETGS, respectively.

427

428 **Triton X-100 membrane extraction**

429 Sporozoites (3 x10^4) were collected and treated with 1.0% Triton X-100 diluted in PBS and
430 incubated on ice for 30 min as previously described (Bergman *et al*, 2003). After incubation,
431 sporozoites were spun at 13,800 × g for 20 min at 4°C. Both treated and untreated sporozoites
432 were washed three times with PBS and fixed with 2% paraformaldehyde diluted in PBS or
433 resuspended.

434

435 **Sporozoite gliding motility assay**

436 To quantify sporozoite gliding motility, a glass eight-well chamber slide was coated with 10
437 µg/ml anti-CSP antibody in PBS overnight, and the assay was performed as described
438 previously (Stewart & Vanderberg, 1988). Hemolymph sporozoites collected in 3%
439 BSA/DMEM were added at 5,000/well and incubated for 1 h at 37°C in a CO2 incubator.
440 After incubation, sporozoites were fixed with 4% PFA, blocked using 3% BSA/PBS, and
441 incubated with biotin-labeled anti-CSP antibody, and signals were revealed using
442 streptavidin-FITC (Invitrogen, USA). Trails associated with sporozoites were counted using a
443 Nikon 80i fluorescence microscope.

444

445 **Immunofluorescence assay**

446

Fixed sporozoites were washed with PBS, permeabilized using 0.1% Triton X-100 for 15 min at room temperature, and then blocked with 1% BSA/PBS for 1 hr at room temperature. Further sporozoites were incubated with anti-mCherry developed in rabbit (Novus Biologicals, USA), anti-CSP mouse monoclonal (Yoshida *et al*, 1980), anti-MTIP, anti-GAP45 or anti-TRAP (Mishra *et al*, 2023) antibodies. The signals were revealed using Alexa Fluor 594-conjugated or Alexa Fluor 488-conjugated antibodies (diluted 1:1,000; Invitrogen, USA). For the staining of EEFs, fixed cultures were washed with PBS, and staining with anti-UIS4 antibody (Mueller *et al*, 2005) was performed as previously described (Narwal *et al*, 2022). Nuclei were stained with Hoechst 33342 (Sigma–Aldrich, USA) and mounted using Prolong diamond anti-fade reagent (Invitrogen, USA). The images were acquired using a confocal laser scanning microscope with a UPlanSAPO 100x/1.4 oil immersion objective (Olympus BX61WI) at 4X magnification.

Western blot analysis

Sporozoites were pelleted by centrifuging at 14,000 rpm for 4 min and resuspended in Laemmli buffer. Immunoblotting was performed as previously described (Narwal *et al*, 2022). Briefly, samples were resolved by SDS-PAGE, transferred to a nitrocellulose membrane (Bio-Rad, USA), and blocked with 1% BSA. The blot was incubated with an anti-mCherry (diluted 1:1,000, Novus Biologicals, USA) or anti-CSP (Yoshida *et al*, 1980) antibodies. The membrane was washed and incubated with HRP-conjugated anti-rabbit or anti-mouse IgG (diluted 1:5,000, Amersham Biosciences, United Kingdom). The signals were detected using ECL chemiluminescent substrate (Thermo Scientific, USA) in a ChemiDoc XRS+ System (Bio-Rad, USA).

Bioinformatic approaches for interrogating protein-protein interactions

To check the interaction of S14 (PBANKA_0605900) with MTIP (PBANKA_1459500) and GAP45 (PBANKA_1437600), in-silico docking was performed. The PDB structures of S14, MTIP and GAP45 are not available, therefore, to obtain their model structure, amino acids sequences were submitted to trRosetta server (https://yanglab.nankai.edu.cn/trRosetta). Obtained structural models were validated using SAVE webserver (https://saves.mbi.ucla.edu/) for Quality factors and Ramachandran plots acceptibility. Models with quality factor above 95% were further processed for the protein-protein interaction studies. ClusPro server (https://cluspro.bu.edu/home.php) was used for initial protein-protein docking studies to predict MTIP-GAP45, MTIP-S14 and S14-GAP45 interaction according to their binding energy. Further, PDB files of the models were submitted to the HDOCK server (http://hdock.phys.hust.edu.cn) for their interaction studies using default parameters. The model with the highest docking score was further used for visualization by Pymol 2.5.4 software (http://www.pymol.org/pymol) (Schrödinger & DeLano).

Yeast two-hybrid interaction studies

The *P. berghei* S14 gene was amplified using primers 2058/2059 and cloned into the Gal4 binding domain-containing vector pAS2 for yeast two-hybrid interaction studies. The MTIP and GAP45 genes were amplified using primer pairs 2060/2061 and 2062/2063, respectively, and cloned into the pGAD-C1 vector in frame with the Gal4 activation domain. These plasmids were cotransformed into *S. cerevisiae* strain PJ69-4A (Clontech, USA), which contains the lacZ gene from *E. coli* encoding β-galactosidase and the HIS3 selectable marker as reporter genes. Interaction studies were performed on SD-leu-trp plates containing X-gal or SD-leu-trp-his plates containing 3-aminotriazole (3-AT). The appearance of blue color on

X-gal plates and growth on plates containing 10 and 25 mM 3-AT in the absence of histidine indicates a positive interaction.

Statistical analysis

Statistical analysis was done using two-tailed, unpaired Student's t test or one-way ANOVA in GraphPad Prism software.

Data and Materials Availability

All data are available within this manuscript, and raw data are available from the corresponding author upon reasonable request. Materials generated in this study are available from the corresponding author on request.

Acknowledgments

We thank Dr. Pratik Narain Srivastava for performing initial bioinformatic studies. We thank BEI Resources, USA, for the parasite strains and plasmids and Dr. Kota Arun Kumar (University of Hyderabad, India) for the pBC-3XHA-mCherry-hDHFR vector. We thank Dr. Photini Sinnis (Johns Hopkins University, USA) for the anti-UIS4 antibody. We acknowledge the THUNDER (BSC0102) and MOES (GAP0118) Intravital and Confocal microscopy facility of CSIR-CDRI. The Council of Scientific and Industrial Research, University Grants Commission, and Indian Council of Medical Research, Government of India research fellowships supported AG, AV, N, RG, SG and SKN. The Ramalingaswami Fellowship grant supported the work (BT/RLF/Re-entry/20/2012). This manuscript is CDRI communication no. 144/2023/SM.

Author contributions

AG, AV and SM conceived the idea, designed and performed the experiments, and analyzed the data. SKN and RG performed the experiments. N completed the in-silico protein-protein interaction studies. SG and SA performed the yeast two-hybrid interaction studies. SM wrote the manuscript, and all the authors have read and approved the manuscript.

Conflict of interest

The authors declare that they have no conflicts of interest.

References

Arredondo SA, Swearingen KE, Martinson T & Steel R (2018) The Micronemal Plasmodium Proteins P36 and P52 Act in Concert to Establish the Compartment Within Infected Hepatocytes. 8: 1–17

Bargieri DY, Andenmatten N, Lagal V, Thiberge S, Whitelaw JA, Tardieux I, Meissner M & Ménard R (2013) Apical membrane antigen 1 mediates apicomplexan parasite attachment but is dispensable for host cell invasion. *Nat Commun* 4

Baum J, Gilberger TW, Frischknecht F & Meissner M (2008) Host-cell invasion by malaria parasites: insights from Plasmodium and Toxoplasma. *Trends Parasitol* 24: 557–563

Baum J, Richard D, Healer J, Rug M, Krnajski Z, Gilberger TW, Green JL, Holder AA & Cowman AF (2006) A conserved molecular motor drives cell invasion and gliding motility across malaria life cycle stages and other apicomplexan parasites. *J Biol Chem* 281: 5197–5208

Bergman LW, Kaiser K, Fujioka H, Coppens I, Daly TM, Fox S, Matuschewski K, Nussenweig V & Kappe SHI (2003) Myosin A tail domain interacting protein (MTIP) localizes to the inner membrane complex of Plasmodium sporozoites. *J Cell Sci* 116: 39–49

Boucher LE & Bosch J (2015) The apicomplexan glideosome and adhesins - Structures and function. *J Struct Biol* 190: 93–114

Buscaglia CA, Coppens I, Hol WGJ & Nussenzweig V (2003) Sites of interaction between aldolase and thrombospondin-related anonymous protein in plasmodium. *Mol Biol Cell* 14: 4947–4957

Choudhary HH, Gupta R & Mishra S (2019) PKAc is not required for the preerythrocytic stages of Plasmodium berghei. 2: 1–11

Combe A, Moreira C, Ackerman S, Thiberge S, Templeton TJ & Ménard R (2009) TREP, a novel protein necessary for gliding motility of the malaria sporozoite. *Int J Parasitol* 39: 489–496

Daher W & Soldati-Favre D (2009) Mechanisms controlling glideosome function in apicomplexans. *Curr Opin Microbiol* 12: 408–414

Douglas RG, Amino R, Sinnis P & Frischknecht F (2015) Active migration and passive transport of malaria parasites. *Trends Parasitol* 31: 357–362

Egarter S, Andenmatten N, Jackson AJ, Whitelaw JA, Pall G, Black JA, Ferguson DJP, Tardieux I, Mogilner A & Meissner M (2014) The toxoplasma Acto-MyoA motor complex is important but not essential for gliding motility and host cell invasion. *PLoS One* 9: e91819

564 Frénal K, Dubremetz JF, Lebrun M & Soldati-Favre D (2017) Gliding motility powers
565 invasion and egress in Apicomplexa. *Nat Rev Microbiol* 15: 645–660
566 Frénal K, Polonais V, Marq JB, Stratmann R, Limenitakis J & Soldati-Favre D (2010)
567 Functional dissection of the apicomplexan glideosome molecular architecture. *Cell Host*
568 *Microbe* 8: 343–357
569 Gaskins E, Gilk S, DeVore N, Mann T, Ward G & Beckers C (2004) Identification of the
570 membrane receptor of a class XIV myosin in Toxoplasma gondii. *J Cell Biol* 165: 383–
571 393
572 Giovannini D, Späth S, Lacroix C, Perazzi A, Bargieri D, Lagal V, Lebugle C, Combe A,
573 Thiberge S, Baldacci P, *et al* (2011) Independent roles of apical membrane antigen 1
574 and rhoptry neck proteins during host cell invasion by apicomplexa. *Cell Host Microbe*
575 10: 591–602
576 Gould SB, Kraft LGK, Van Dooren GG, Goodman CD, Ford KL, Cassin AM, Bacic A,
577 McFadden GI & Waller RF (2011) Ciliate pellicular proteome identifies novel protein
578 families with characteristic repeat motifs that are common to alveolates. *Mol Biol Evol*
579 28: 1319–1331
580 Gupta R, Mishra A, Choudhary HH, Narwal SK, Nayak B, Srivastava PN & Mishra S (2020)
581 Secreted protein with altered thrombospondin repeat (SPATR) is essential for asexual
582 blood stages but not required for hepatocyte invasion by the malaria parasite
583 Plasmodium berghei. *Mol Microbiol* 113: 478–491
584 Harding CR, Egarter S, Gow M, Jiménez-Ruiz E, Ferguson DJP & Meissner M (2016)
585 Gliding Associated Proteins Play Essential Roles during the Formation of the Inner
586 Membrane Complex of Toxoplasma gondii. *PLoS Pathog* 12: e1005403
587 Heintzelman MB (2015) Gliding motility in apicomplexan parasites. *Semin Cell Dev Biol* 46:
588 135–142
589 Heiss K, Nie H, Kumar S, Daly TM, Bergman LW & Matuschewski K (2008) Functional
590 characterization of a redundant Plasmodium TRAP family invasin, TRAP-like protein,
591 by aldolase binding and a genetic complementation test. *Eukaryot Cell* 7: 1062–1070
592 Huynh M & Carruthers VB (2006) Toxoplasma MIC2 Is a Major Determinant of Invasion
593 and Virulence. 2
594 Ishino T, Chinzei Y & Yuda M (2005a) Two proteins with 6-cys motifs are required for
595 malarial parasites to commit to infection of the hepatocyte. *Mol Microbiol* 58: 1264–
596 1275
597 Ishino T, Chinzei Y & Yuda M (2005b) A Plasmodium sporozoite protein with a membrane
598 attack complex domain is required for breaching the liver sinusoidal cell layer prior to
599 hepatocyte infection. *Cell Microbiol* 7: 199–208
600 Ishino T, Yano K, Chinzei Y & Yuda M (2004) Cell-passage activity is required for the
601 malarial parasite to cross the liver sinusoidal cell layer. *PLoS Biol* 2: E4
602 Janse CJ, Ramesar J & Waters AP (2006) High-efficiency transfection and drug selection of
603 genetically transformed blood stages of the rodent malaria parasite Plasmodium
604 berghei. *Nat Protoc* 1: 346–356
605 Jewett TJ & Sibley LD (2003) Aldolase forms a bridge between cell surface adhesins and the
606 actin cytoskeleton in apicomplexan parasites. *Mol Cell* 11: 885–894
607 Kaiser K, Camargo N & Kappe SHI (2003) Transformation of sporozoites into early
608 exoerythrocytic malaria parasites does not require host cells. *J Exp Med* 197: 1045–1050
609 Kaiser K, Matuschewski K, Camargo N, Ross J & Kappe SHI (2004) Differential
610 transcriptome profiling identifies Plasmodium genes encoding pre-erythrocytic stage-
611 specific proteins. *Mol Microbiol* 51: 1221–1232
612 Kariu T, Yuda M, Yano K & Chinzei Y (2002) MAEBL is essential for malarial sporozoite
613 infection of the mosquito salivary gland. *J Exp Med* 195: 1317–1323

614 Kehrer J, Singer M, Lemgruber L, Silva PAGC, Frischknecht F & Mair GR (2016) A
615 Putative Small Solute Transporter Is Responsible for the Secretion of G377 and TRAP-
616 Containing Secretory Vesicles during Plasmodium Gamete Egress and Sporozoite
617 Motility. 1–25
618 King CA (1988) Cell motility of sporozoan protozoa. *Parasitol Today* 4: 315–319
619 Klug D & Frischknecht F (2017) Motility precedes egress of malaria parasites from oocysts.
620 *Elife* 6: 1–32
621 Kono M, Prusty D, Parkinson J & Gilberger TW (2013) The apicomplexan inner membrane
622 complex. *Front Biosci (Landmark Ed* 18: 982–992
623 Labaied M, Camargo N & Kappe SHII (2007) Depletion of the Plasmodium berghei
624 thrombospondin-related sporozoite protein reveals a role in host cell entry by
625 sporozoites. *Mol Biochem Parasitol* 153: 158–166
626 Loubens M, Marinach C, Paquereau C & Hamada S (2023) The claudin-like apicomplexan
627 microneme protein is required for gliding motility and infectivity of Plasmodium
628 sporozoites. 1–24
629 Manzoni G, Marinach C, Topçu S, Briquet S, Grand M, Tolle M, Gransagne M, Lescar J,
630 Andolina C, Franetich JF, *et al* (2017) Plasmodium P36 determines host cell receptor
631 usage during sporozoite invasion. *Elife* 6: 1–24
632 Mastan BS, Narwal SK, Dey S, Kumar KA & Mishra S (2017) Plasmodium berghei
633 plasmepsin VIII is essential for sporozoite gliding motility. *Int J Parasitol* 47: 239–245
634 Meissner M, Ferguson DJP & Frischknecht F (2013) Invasion factors of apicomplexan
635 parasites: essential or redundant? *Curr Opin Microbiol* 16: 438–444
636 Mikolajczak SA, Silva-Rivera H, Peng X, Tarun AS, Camargo N, Jacobs-Lorena V, Daly
637 TM, Bergman LW, de la Vega P, Williams J, *et al* (2008) Distinct Malaria Parasite
638 Sporozoites Reveal Transcriptional Changes That Cause Differential Tissue Infection
639 Competence in the Mosquito Vector and Mammalian Host. *Mol Cell Biol* 28: 6196–
640 6207
641 Mishra A, Srivastava PN, H SA & Mishra S (2023) Autophagy protein Atg7 is essential and
642 druggable for maintaining malaria parasite cellular homeostasis and organelle
643 biogenesis. *bioRxiv*: 2023.08.16.553492
644 Mueller AK, Camargo N, Kaiser K, Andorfer C, Frevert U, Matuschewski K & Kappe SHI
645 (2005) Plasmodium liver stage developmental arrest by depletion of a protein at the
646 parasite-host interface. *Proc Natl Acad Sci U S A* 102: 3022–3027
647 Narwal SK, Nayak B, Mehra P & Mishra S (2022) Protein kinase 9 is not required for
648 completion of the Plasmodium berghei life cycle. *Microbiol Res* 260: 127051
649 Opitz C & Soldati D (2002) 'The glideosome': a dynamic complex powering gliding motion
650 and host cell invasion by Toxoplasma gondii. *Mol Microbiol* 45: 597–604
651 Perrin AJ, Collins CR, Russell MRG, Collinson LM, Baker DA & Blackman MJ (2018) The
652 actinomyosin motor drives malaria parasite red blood cell invasion but not egress. *MBio*
653 9: 1–13
654 Poulin B, Patzewitz E-M, Brady D, Silvie O, Wright MH, Ferguson DJP, Wall RJ, Whipple
655 S, Guttery DS, Tate EW, *et al* (2013) Unique apicomplexan IMC sub-compartment
656 proteins are early markers for apical polarity in the malaria parasite. *Biol Open* 2: 1160–
657 1170
658 Prudêncio M, Rodriguez A & Mota MM (2006) The silent path to thousands of merozoites:
659 The Plasmodium liver stage. *Nat Rev Microbiol* 4: 849–856
660 Rees-Channer RR, Martin SR, Green JL, Bowyer PW, Grainger M, Molloy JE & Holder AA
661 (2006) Dual acylation of the 45 kDa gliding-associated protein (GAP45) in Plasmodium
662 falciparum merozoites. *Mol Biochem Parasitol* 149: 113–116
663 Rénia L, Miltgen F, Charoenvit Y, Ponnudurai T, Verhave JP, Collins WE & Mazier D

(1988) Malaria sporozoite penetration A new approach by double staining. *J Immunol Methods* 112: 201–205

Ripp J, Kehrer J, Smyrnakou X, Tisch N, Tavares J, Amino R, Ruiz de Almodovar C & Frischknecht F (2021) Malaria parasites differentially sense environmental elasticity during transmission. *EMBO Mol Med* 13: 1–10

Risco-Castillo V, Topçu S, Marinach C, Manzoni G, Bigorgne AE, Briquet S, Baudin X, Lebrun M, Dubremetz J-F & Silvie O (2015) Malaria Sporozoites Traverse Host Cells within Transient Vacuoles. *Cell Host Microbe* 18: 593–603

Saenz FE, Balu B, Smith J, Mendonca SR & Adams JH (2008) The transmembrane isoform of Plasmodium falciparum MAEBL is essential for the invasion of Anopheles salivary glands. *PLoS One* 3

Schrödinger LLC & DeLano W PyMOL. [PREPRINT]

Sebastian S, Brochet M, Collins MO, Schwach F, Jones ML, Goulding D, Rayner JC, Choudhary JS & Billker O (2012) A Plasmodium calcium-dependent protein kinase controls zygote development and transmission by translationally activating repressed mRNAs. *Cell Host Microbe* 12: 9–19

Srivastava PN & Mishra S (2022) Disrupting a Plasmodium berghei putative phospholipase impairs efficient egress of merosomes. *Int J Parasitol* 52: 547–558

Steinbuechel M & Matuschewski K (2009) Role for the Plasmodium sporozoite-specific transmembrane protein S6 in parasite motility and efficient malaria transmission. *Cell Microbiol* 11: 279–288

Stewart MJ & Vanderberg JP (1988) Malaria sporozoites leave behind trails of circumsporozoite protein during gliding motility. *J Protozool* 35: 389–393

Sultan AA, Thathy V, Frevert U, Robson KJ, Crisanti A, Nussenzweig V, Nussenzweig RS & Ménard R (1997) TRAP is necessary for gliding motility and infectivity of plasmodium sporozoites. *Cell* 90: 511–522

Talman AM, Lacroix C, Marques SR, Blagborough AM, Carzaniga R, Ménard R & Sinden RE (2011) PbGEST mediates malaria transmission to both mosquito and vertebrate host. 82: 462–474

Togbe D, de Sousa PL, Fauconnier M, Boissay V, Fick L, Scheu S, Pfeffer K, Menard R, Grau GE, Doan BT, *et al* (2008) Both functional LTβ receptor and TNF receptor 2 are required for the development of experimental cerebral malaria. *PLoS One* 3

Yeoman JA, Hanssen E, Maier AG, Klonis N, Maco B, Baum J, Turnbull L, Whitchurch CB, Dixon MWA & Tilley L (2011) Tracking Glideosome-Associated Protein 50 Reveals the Development and Organization of the Inner Membrane Complex of. 10: 556–564

Yoshida N, Nussenzweig RS, Potocnjak P, Nussenzweig V & Aikawa M (1980) Hybridoma Produces Protective Antibodies Directed against the Sporozoite Stage of Malaria Parasite. *Science (80-)* 207: 71–73

Table 1. Infectivity of *S14* KO sporozoites in C57BL/6 mice. C57BL/6 mice were inoculated with WT GFP, *S14* KO or *S14* comp sporozoites by mosquito bite or intravenous injection. The appearance of parasites in the blood was confirmed by making Giemsa-stained blood smear.

Experiment	Parasites	Route	Number of sporozoites injected	Mice positive/Mice infected	Pre-patent period (days)
1	WT GFP	Mosquito bite	From 10 mosquitos	4/4	3
	S14 KO c1	Mosquito bite	From 10 mosquitos	0/4	NA
	S14 KO c2	Mosquito bite	From 10 mosquitos	0/4	NA
2	WT GFP	intravenous	5,000	5/5	3
	S14 comp	intravenous	5,000	5/5	3
	S14 KO c1	intravenous	5,000	0/5	NA
	S14 KO c2	intravenous	5,000	0/5	NA
	S14 KO (yFCU)	intravenous	5,000	0/5	NA
3	WT GFP	intravenous	5,000	0/4	3
	S14 KO c1	intravenous	5,000	0/4	NA
	S14 KO c2	intravenous	5,000	0/4	NA

741 **Figure legends**

742 **Figure 1. *S14* expression and localization. (A)** The gene expression of *S14* was analyzed
743 using quantitative real-time PCR, which revealed the highest expression in sporozoites. The
744 expression of *S14* was normalized to the *PbHsp70* transcript. BS; blood stages, Schz;
745 schizonts, MG Spz; midgut sporozoites, SG Spz; salivary gland sporozoites, LS; liver stages.
746 **(B)** Live microscopy image of midgut oocysts expressing the mCherry reporter. **(C)**
747 mCherry-expressing salivary gland sporozoites. **(D)** Salivary gland sporozoites expressing
748 S14-3XHA-mCherry on the membrane. **(E)** Confirmation of S14 expression on the
749 membrane of the sporozoites by coimmunostaining with surface protein marker anti-CSP
750 antibody. **(F)** Western blot analysis of S14-3XHA-mCherry salivary gland sporozoite lysates.
751 The blot was first probed with an anti-mCherry antibody, then stripped and reprobed with an
752 anti-CSP antibody.

753

754 **Figure 2. S14 is essential for salivary gland invasion by sporozoites. (A)** Live microscopy
755 images of the mosquito midgut showing oocysts. **(B)** The number of oocysts in WT GFP and
756 *S14* KO parasites was not significantly different (P= 0.952, one-way ANOVA). **(C)** Live
757 microscopy images of sporulating oocysts of WT GFP and *S14* KO parasites. **(D)** Midgut
758 oocyst sporozoite number, no significant difference (P= 0.943, one-way ANOVA). **(E)**
759 Dissected salivary glands showed GFP-expressing sporozoites in WT GFP, while no GFP-
760 expressing sporozoites were observed in *S14* KO. **(F)** Salivary gland sporozoite numbers,
761 negligible sporozoites in *S14* KO, a significant difference (***P<0.0008, one-way ANOVA).
762 Complementation restored the sporozoites number in *S14* KO parasites at the WT GFP
763 levels, no significant difference (P= 0.434, Student's t test) **(G)** *S14* KO and WT GFP
764 hemolymph sporozoites were collected on the indicated days post blood meal, and sporozoite
765 numbers were quantified. We found a comparable number of sporozoites on day 15, with no

766 significant difference (P=0.621). There was a higher accumulation of hemolymph sporozoites
767 in S14 KO on days 17-23 with a significant difference from WT GFP (day 19 *P=0.0187,
768 day 17 ***P<0.0001, days 21 and 23 ***P=0.0006, one-way ANOVA).

769 **Figure 3. S14 is essential for hepatocyte invasion and malaria transmission. (A)** HepG2
770 cells infected with hemolymph sporozoites were immunostained, and EEF numbers were
771 quantified. No EEFs were observed in *S14* KO parasites, a significant difference
772 (***P<0.0001, one-way ANOVA). **(B)** Quantification of sporozoites inside vs outside in
773 invasion assay. All sporozoites were found to be outside in *S14* KO parasites, a significant
774 difference (***P<0.0001, one-way ANOVA). **(C)** *S14* KO and WT GFP hemolymph
775 sporozoites transformed into bulbs after incubation for 4 h in an activation medium. **(D)**
776 Quantifying sporozoite transformation into bulbs, no significant difference (P=0.419, one-
777 way ANOVA).

778

779 **Figure 4. S14 is an inner membrane protein and is essential for parasite gliding motility.**
780 **(A)** Triton X-100-treated sporozoites retained mCherry staining, which colocalized with
781 MTIP and GAP45, while CSP staining was lost, suggesting that S14 is present within the
782 inner membrane of the sporozoites. **(B)** Triton X-100-treated and untreated sporozoites were
783 denatured in SDS-PAGE sample buffer and resolved on SDS-PAGE. The blot was probed
784 with an anti-mCherry antibody, then stripped and reprobed with an anti-CSP antibody.
785 Detection of the mCherry signal in Triton X-100-treated sporozoites confirmed its presence
786 on the inner membrane. S14 Tr; S14-3XHA-mCherry transgenic parasite. **(C)** The WT GFP
787 and *S14* KO hemolymph sporozoites were allowed to glide for one hour, and the CSP trail
788 left was revealed using a biotin-CSP antibody followed by streptavidin-FITC. All *S14* KO
789 sporozoites were nonmotile. **(D)** Gliding was quantified by counting the CSP trials, and a
790 significant difference was observed (***P<0.0003, one-way ANOVA).

Figure 5: In silico docking studies using HDOCK server showing binding of *P. berghei* S14-MTIP, MTIP-GAP45 and S14-GAP45. A list of receptor-ligand interface are given in Table S4. Images were visualized using Pymol 2.5.4 software. **(A)** S14-MTIP interacting receptor ligand residues (228A CYS-4A GLN, 230A ASN-142A GLU, 231A TYR-4A GLN, 233A CYS-4A GLN, 235A ALA-1A MET). **(B)** MTIP-GAP45 interacting receptor ligand residues (7A MET -97A ASP, 10A PHE-101A THR, 149A ALA-105A LEU, 152A ASP- 108A SER, 255A THR- 107A LEU, 157A GLY- 112A THR). **(C)** S14-GAP45 interacting receptor ligand residues (231A TYR-135A LYS, 233A CYS- 134A TYR, 237A VAL-133A THR, 246A TYR-130A ILE, 248A TYR- 131A TYR).

Figure 6. S14 interacts with GAP45 and MTIP in a yeast two-hybrid assay. The S14, MTIP, and GAP45 genes were cloned in a yeast two-hybrid vector. The interaction was analyzed using LacZ as a reporter gene on SD-trp-leu plates containing X-gal and the his3+ marker as a reporter gene on SD-trp-leu plates lacking histidine. 3AT was used to prevent any leaky expression of the his3 marker gene.

Figure 7. S14 does not affect IMC and surface protein expression and localization. WT GFP and *S14* KO hemolymph sporozoites were spotted on a 12-well slide and air-dried. Immunostaining with anti-GAP45, anti-MTIP, anti-CSP, and anti-TRAP antibodies revealed similar expression and localization in WT GFP and *S14* KO sporozoites.

Figure 8. A schematic model of sporozoite membrane with S14. The sporozoite membrane is shown with surface proteins TRAP and CSP. We show that S14 interacts with MTIP and GAP45 and coordinates gliding motility by connecting these two proteins.

Figure 1

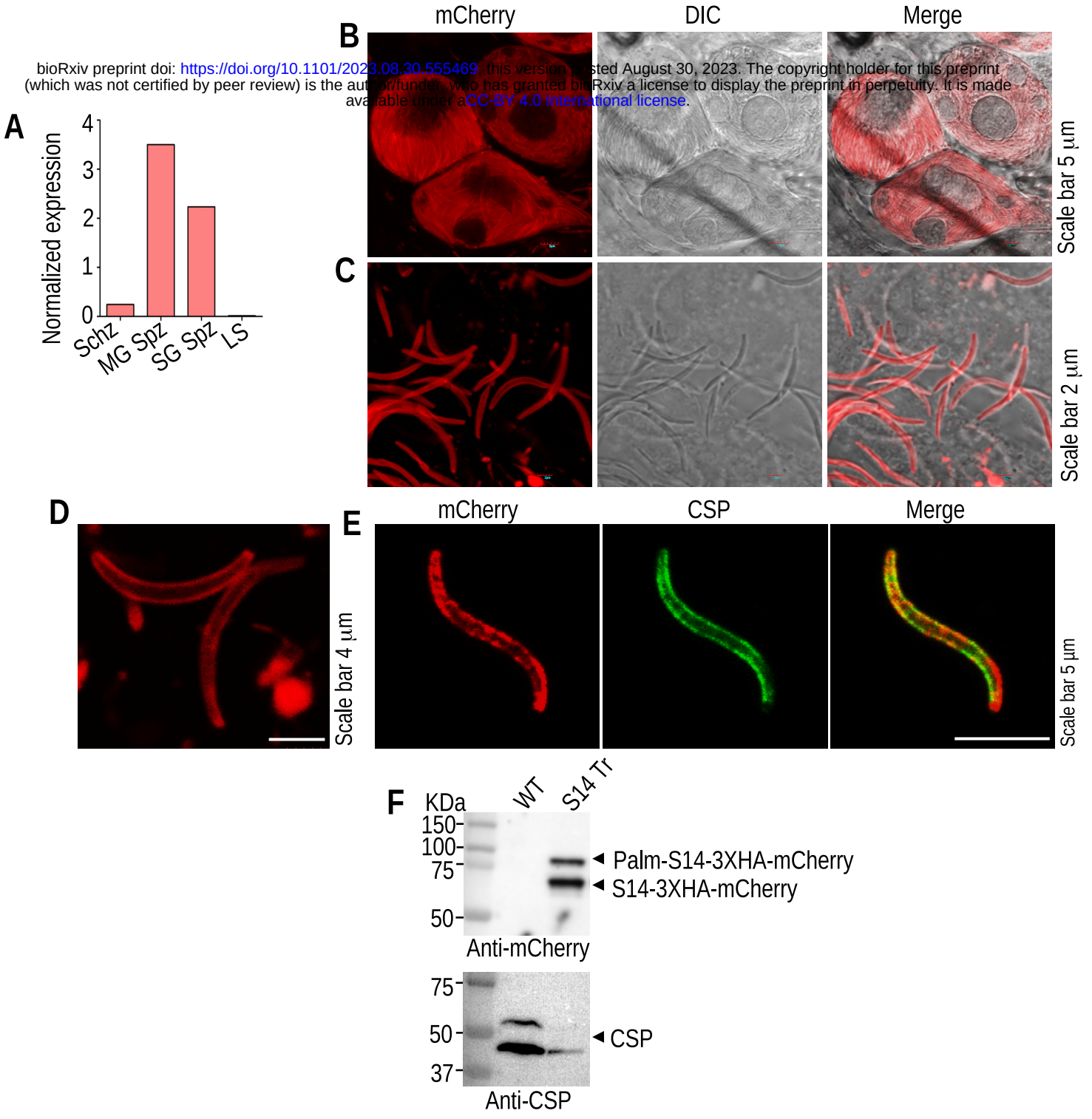

Figure 2

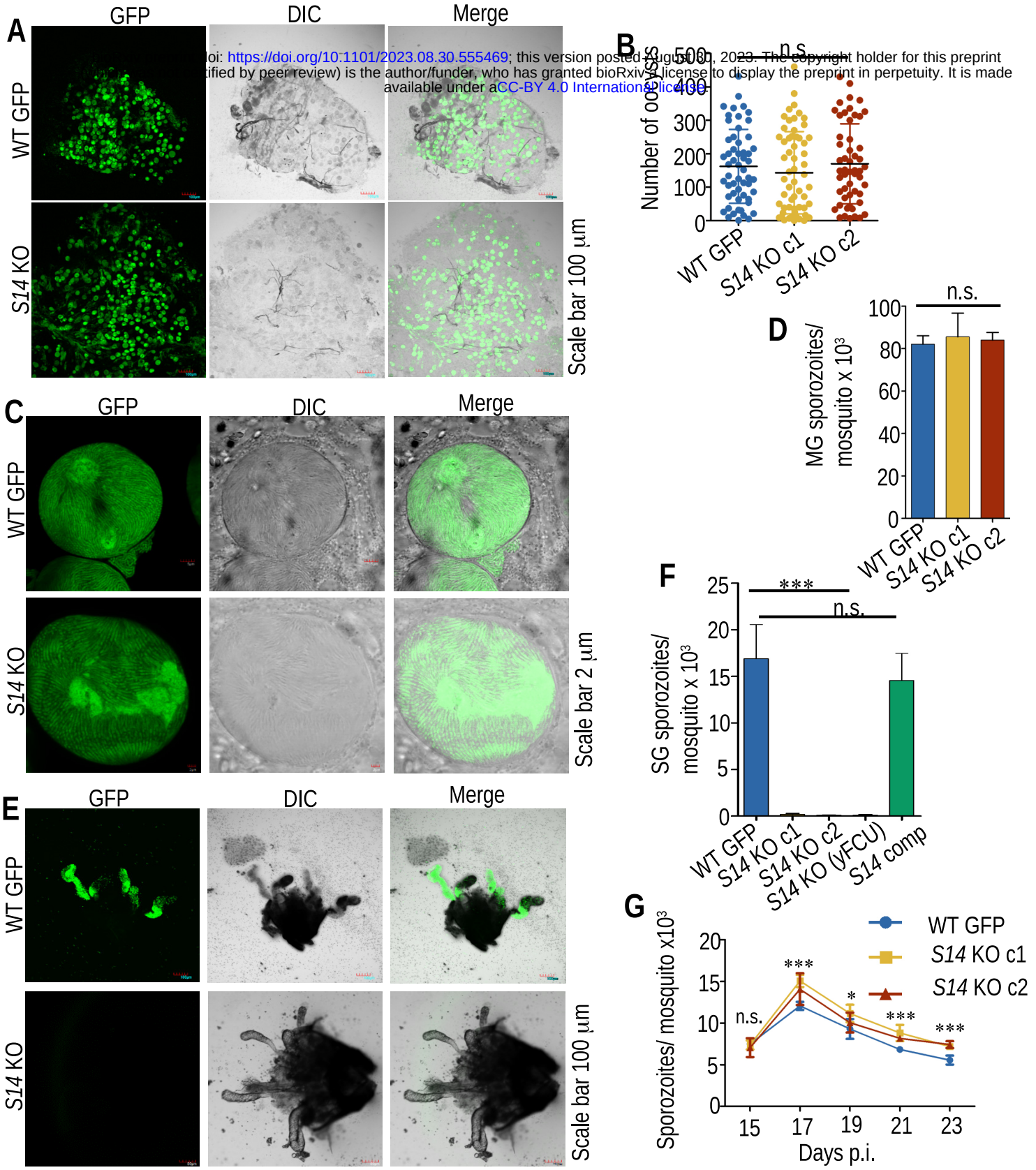

Figure 3

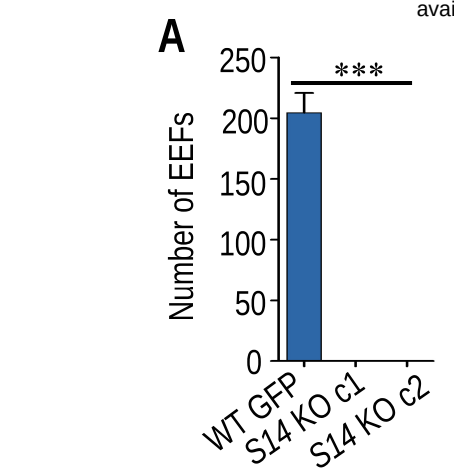

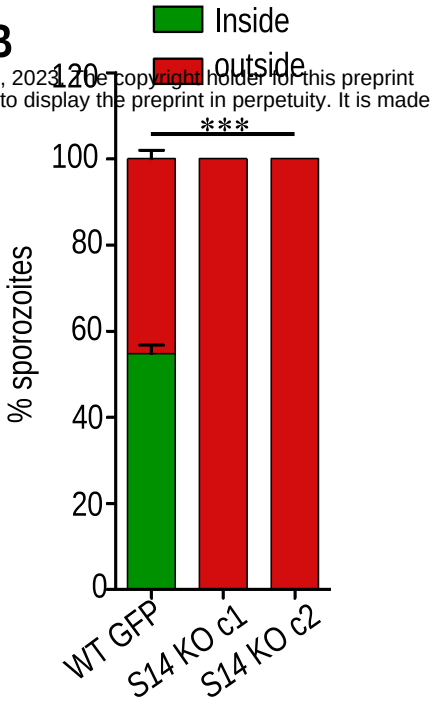

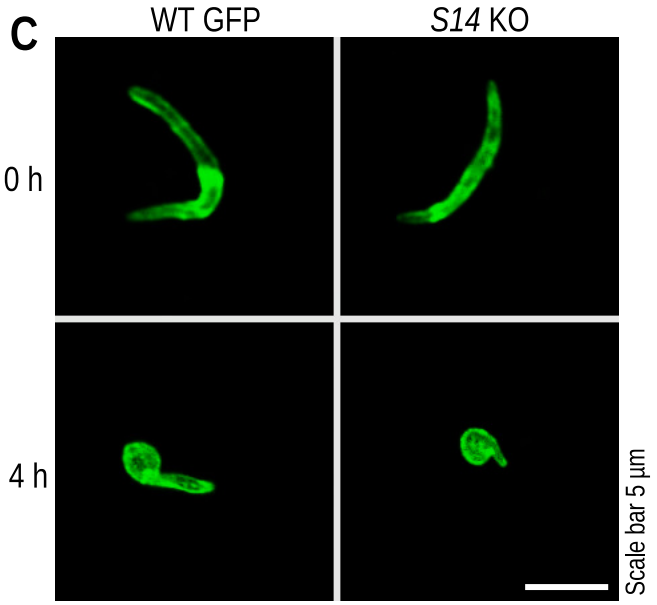

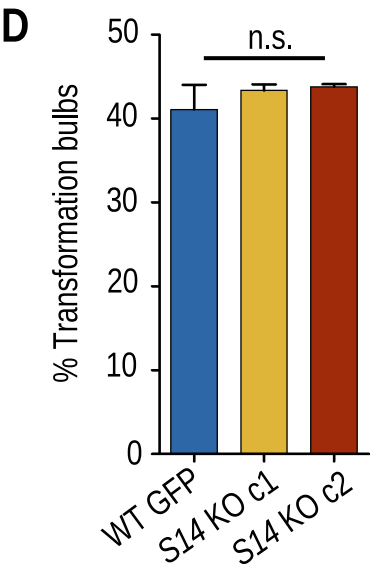

Figure 4

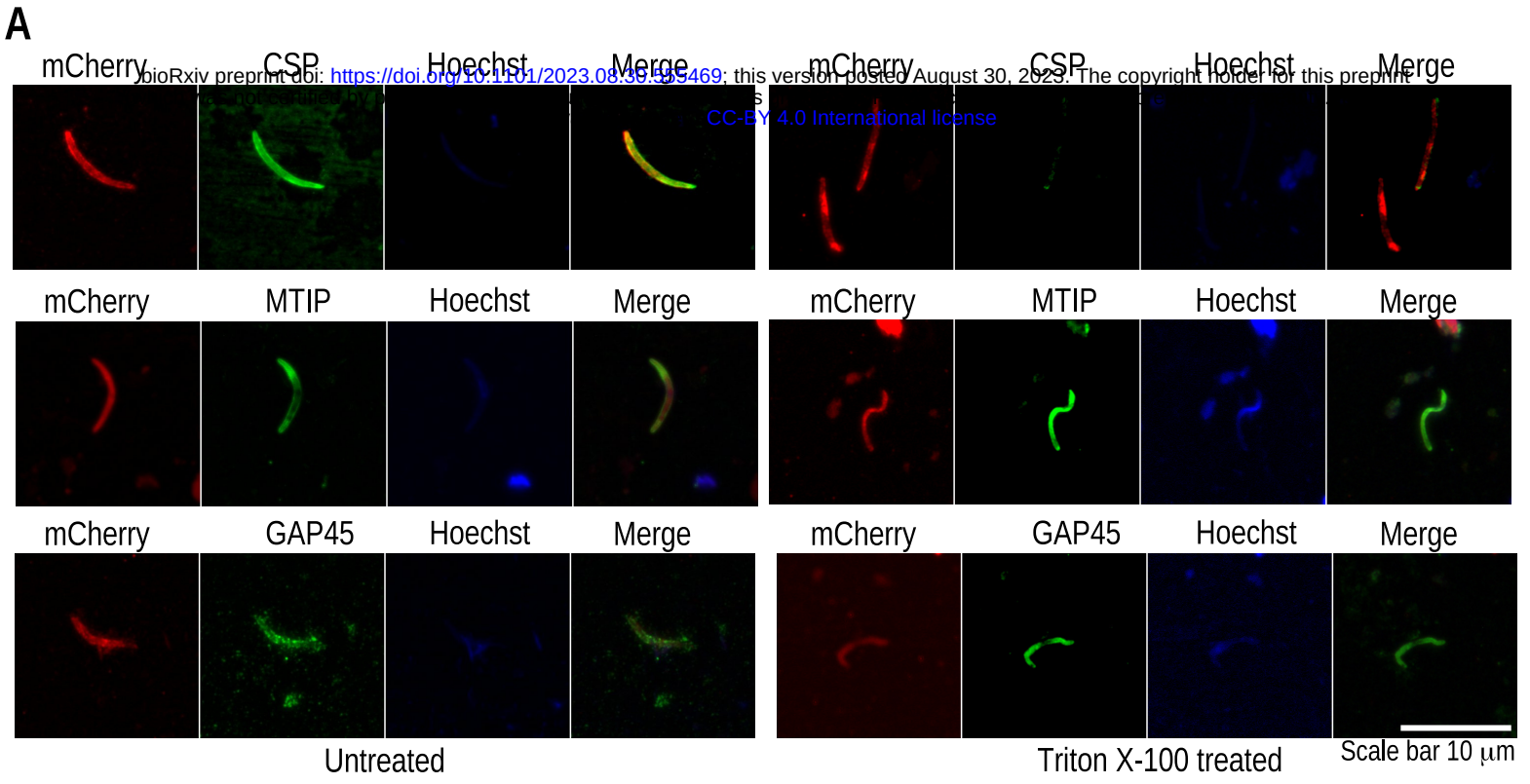

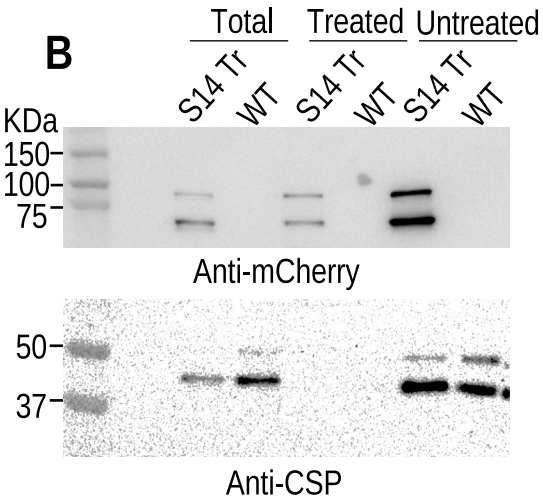

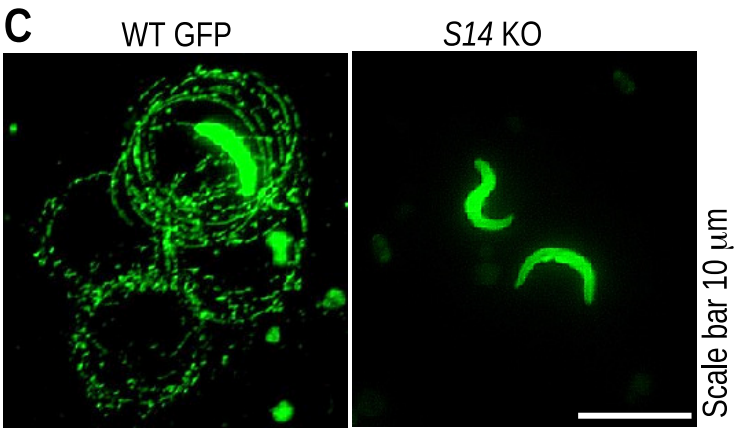

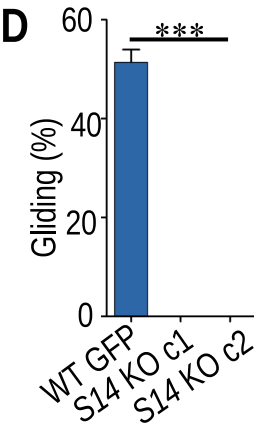

Figure 5

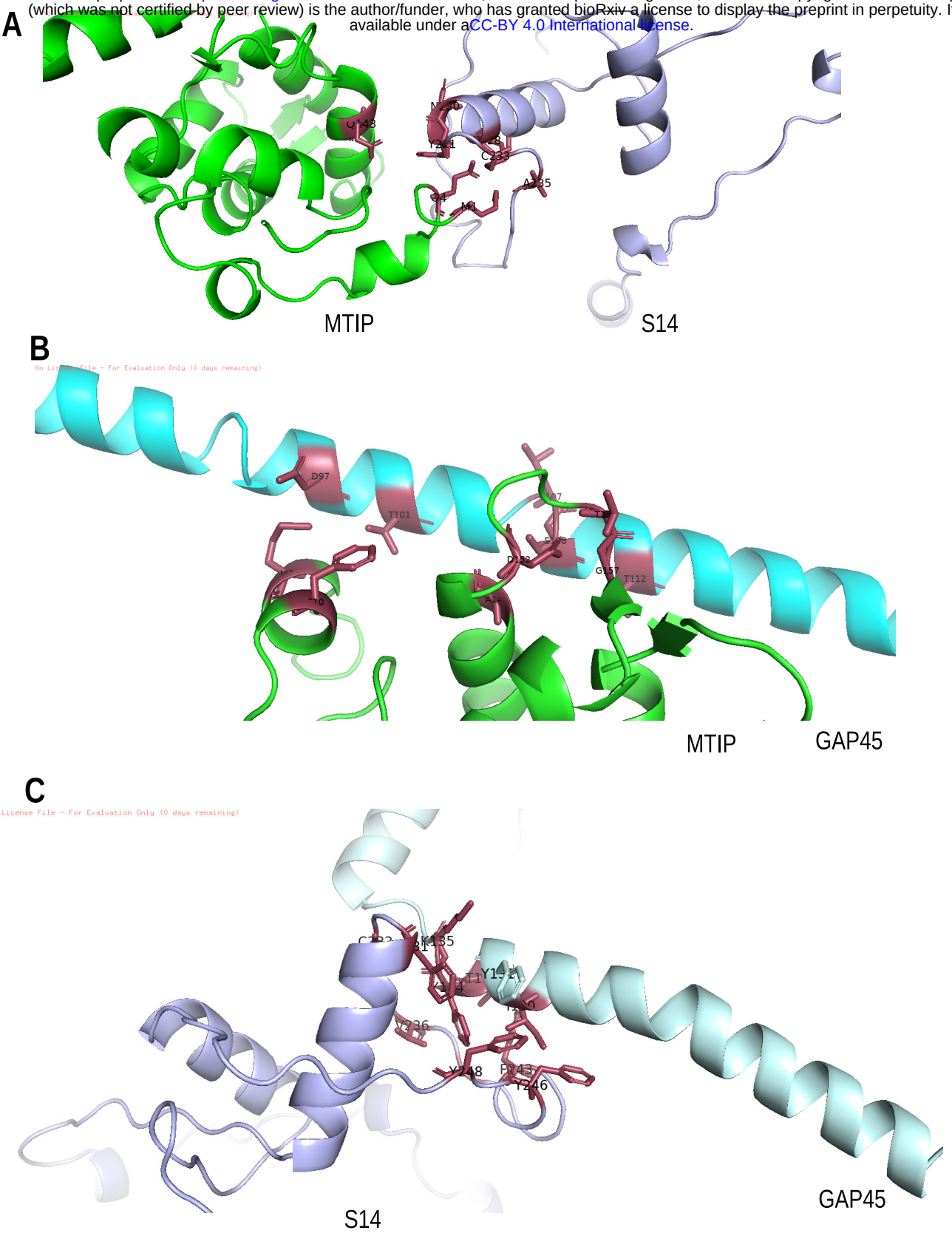

Figure 6

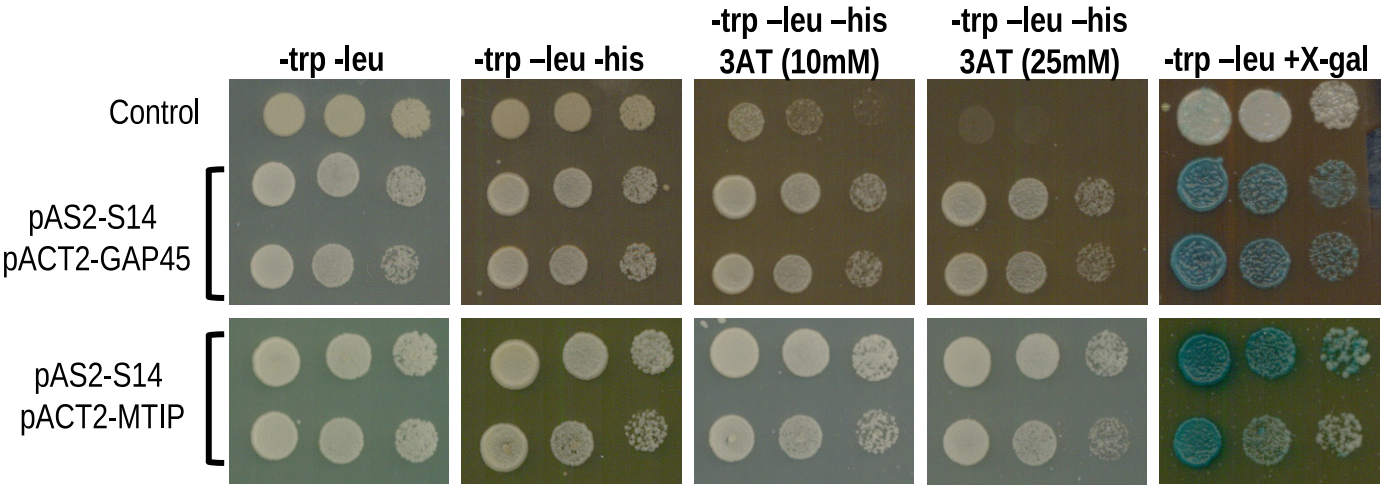

Figure 7

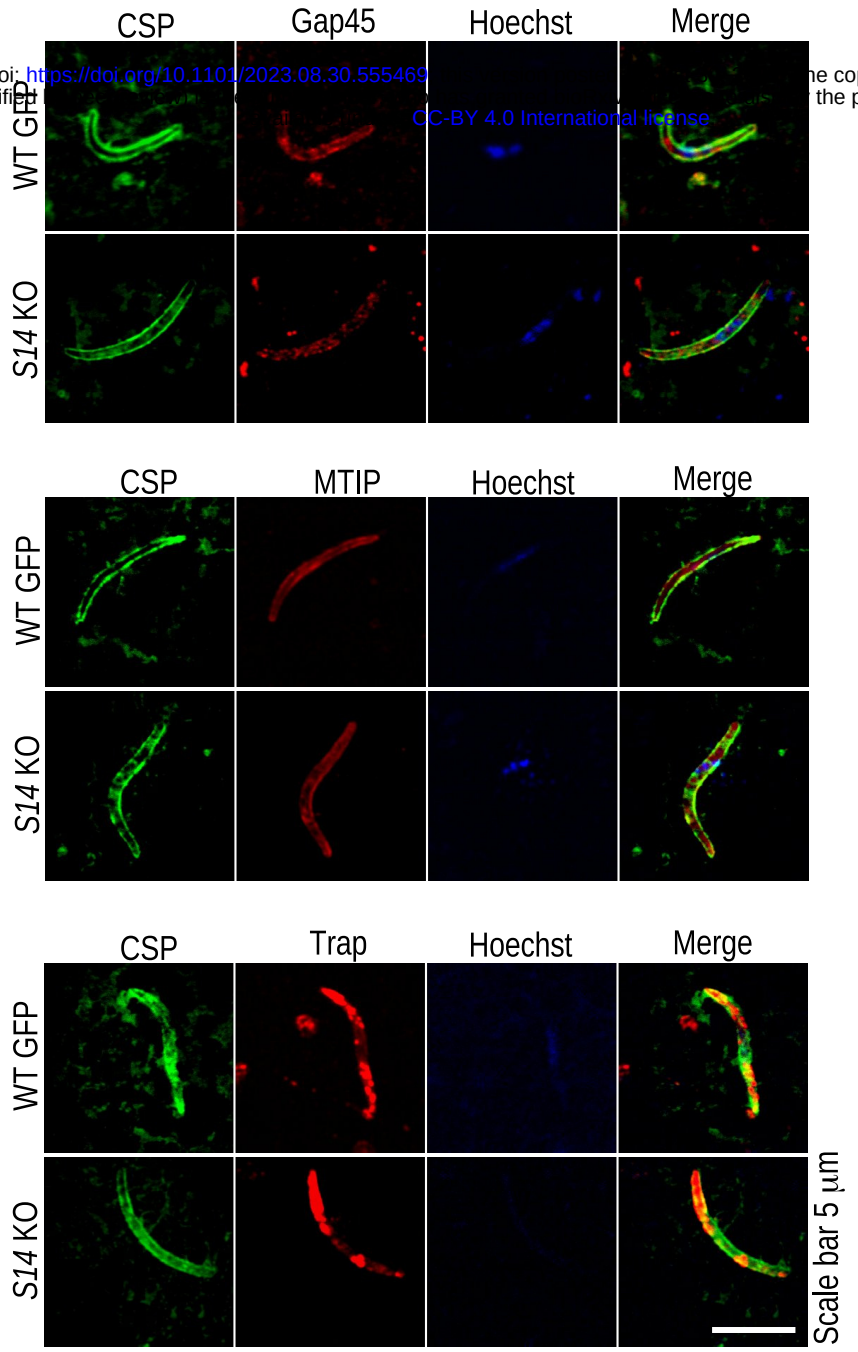

Figure 8